

## Quenching of single-particle strengths in direct reactions

J. Manfredi<sup>1,2,\*</sup>, J. Lee,<sup>3</sup> A. M. Rogers,<sup>4</sup> M. B. Tsang,<sup>1,2</sup> W. G. Lynch,<sup>1,2</sup> C. Anderson,<sup>1</sup> J. Barney,<sup>1,2</sup> K. W. Brown,<sup>1,5</sup> B. Brophy,<sup>1</sup> G. Cerizza,<sup>1</sup> Z. Chajecski,<sup>6</sup> G. Chen,<sup>6</sup> J. Elson,<sup>5</sup> J. Estee,<sup>1,2</sup> H. Iwasaki,<sup>1,2</sup> C. Langer,<sup>1,7</sup> Z. Li,<sup>8</sup> C. Loelius,<sup>1,2</sup> C. Y. Niu,<sup>1,8</sup> C. Pruitt,<sup>5</sup> H. Setiawan,<sup>1,2</sup> R. Showalter,<sup>1,2</sup> K. Smith,<sup>9</sup> L. G. Sobotka,<sup>5</sup> S. Sweany,<sup>1,2</sup> S. Tangwancharoen,<sup>1,2</sup> J. R. Winkelbauer,<sup>1,2</sup> Z. Xiao,<sup>10</sup> and Z. Xu<sup>3</sup>

<sup>1</sup>National Superconducting Cyclotron Laboratory, Michigan State University, East Lansing, Michigan 48824, USA

<sup>2</sup>Department of Physics and Astronomy, Michigan State University, East Lansing, Michigan 48824, USA

<sup>3</sup>Department of Physics, The University of Hong Kong, Pokfulam Road, Hong Kong, China

<sup>4</sup>Department of Physics, University of Massachusetts Lowell, Lowell, Massachusetts 01854, USA

<sup>5</sup>Department of Chemistry, Washington University, St. Louis, Missouri 63130, USA

<sup>6</sup>Department of Physics, Western Michigan University, Kalamazoo, Michigan 49008, USA

<sup>7</sup>FH Aachen University of Applied Sciences, 52066 Aachen, Germany

<sup>8</sup>School of Physics and State Key Laboratory of Nuclear Physics and Technology, Peking University, Beijing 100871, China

<sup>9</sup>Department of Physics and Astronomy, University of Tennessee, Knoxville, Tennessee 37996, USA

<sup>10</sup>Department of Physics, Tsinghua University, Beijing 100084, China



(Received 19 June 2020; revised 9 November 2020; accepted 8 June 2021; published 9 August 2021)

A discrepancy in the asymmetry dependence of spectroscopic factors extracted with different reaction probes calls into question whether the corresponding reaction models are properly understood. In this work, we present extracted spectroscopic factors from the  $^{46,34}\text{Ar}(p, d)^{45,33}\text{Ar}$  transfer reactions in inverse kinematics at a beam energy of 70 MeV/nucleon. The results are consistent with previous measurements of these reactions at a lower beam energy [Lee *et al.*, *Phys. Rev. Lett.* **104**, 112701 (2010)], indicating that the transfer reaction is a reliable probe for the nuclear structure of exotic nuclei across a wide energy range. Results from a large body of transfer reaction measurements,  $(p, pN)$  measurements, and theoretical nuclear structure studies make a compelling case for much weaker asymmetry dependence than what is observed with single-nucleon knockout reactions on beryllium or carbon targets.

DOI: [10.1103/PhysRevC.104.024608](https://doi.org/10.1103/PhysRevC.104.024608)

### I. INTRODUCTION

Atomic nuclei consist of interacting fermions. Correlations between individual nucleons modify the single-particle model that assumes nucleons move in a mean-field potential provided by the other nucleons [1,2]. Short-range correlations arising from strong repulsion at small distances push nucleons to higher momentum single-particle orbitals [1,3], while long-range correlations between valence nucleons lead to collective behavior [4]. The *spectroscopic factor* (SF) quantifies the occupancy of a given single-particle orbital in a particular nuclear state, and can be studied with cross-section measurements of direct reactions that remove or add single nucleons. Measurements of a variety of nuclear reactions on stable isotopes across a wide mass range show consistent SF reduction to around 60–70% of independent-particle model expectations [5–8]. Although isolated SF measurements can fluctuate with model inputs, previous work has shown that a systematic approach across multiple systems yields consistent results [7–12].

The study of nuclei far from the valley of stability requires reaction techniques that use inverse kinematics with rare isotope beams, such as single-nucleon transfer, single-nucleon beryllium-induced knockout, and quasifree knockout [8,13,14]. There is disagreement among these techniques on the degree of SF quenching as a function of nuclear asymmetry, parametrized by the difference in neutron and proton separation energies  $\Delta S$ . Intermediate-energy measurements (mostly between 80 and 100 MeV/nucleon) of single-nucleon knockout induced by beryllium or carbon targets indicate that the SFs of the minority nucleons in asymmetric systems are strongly reduced relative to shell-model expectations [8,15–18]. However, low-energy transfer measurements of exotic species consistently show at most a weak dependence on  $\Delta S$  [19–22]. Recent quasifree knockout [both  $(p, 2p)$  and  $(p, pn)$ ] measurements have provided further evidence for a flat or weak asymmetry dependence [14,23–25]. Electron scattering measurements on stable nuclei show that short-range correlations more strongly affect minority nucleons [26], but recent theoretical calculations suggest that this manifests in exotic nuclei as a weak asymmetry dependence [27].

The disagreement between transfer and Be/C-induced knockout reactions indicates incomplete theoretical

\*juan.manfredi@afit.edu

understanding of the reaction mechanisms. This inconsistency is impactful, as each of these methods is used in a wide variety of nuclear physics experiments [28,29]. Transfer reaction measurements at higher beam energies can serve as a test of consistency of the transfer reaction technique, as well as a bridge to enable direct comparison between results from low-energy transfer and those from Be/C-induced knockout measurements at medium energy. The existing transfer measurements at high energies are only on nuclei near stability [30,31].

In this article we present reduction factors extracted from the  $^{34}\text{Ar}(p, d)$  and  $^{46}\text{Ar}(p, d)$  transfer reactions measured at a significantly higher beam energy (70 MeV/nucleon) than in the previous measurement reported in Ref. [19]. Agreement on the strength of the asymmetry dependence between this higher-energy measurement and that of Lee *et al.* [19] would reaffirm the consistency of the transfer method across a wide energy range at high asymmetry. Disagreement between these two measurements would indicate a potential problem with the current understanding of the single-nucleon transfer mechanism for deeply bound nucleons. Another motivation to test the consistency of  $(p, d)$  measurements for asymmetric systems at different energies is that the upcoming Facility for Rare Isotope Beams will expand the range of possible transfer reaction measurements, in particular at high beam energy where rates are higher. We present our results, as well as a systematic comparison of asymmetry trends from several experimental and theoretical studies that support a weaker asymmetry dependence than what is observed in Be/C-induced knockout experiments. This discrepancy of the reduction factor remains a key problem in reaction theory that urgently needs to be resolved.

## II. TRANSFER-REACTION CROSS SECTIONS

The differential cross sections of the  $^{46}\text{Ar}(p, d)^{45}\text{Ar}$  and  $^{34}\text{Ar}(p, d)^{33}\text{Ar}$  single-neutron transfer reactions at 70 MeV/nucleon were measured at the National Superconducting Cyclotron Laboratory at Michigan State University [32]. Both measurements were kinematically complete, meaning that both the deuteron and the heavy residue were detected. The  $^{46}\text{Ar}$  and  $^{34}\text{Ar}$  beams were impinged on  $\text{CH}_2$  targets of 75- and 25- $\mu\text{m}$  thickness, respectively. Outgoing deuterons were detected with the High Resolution Array (HiRA) [33] in coincidence with heavy reaction residues detected in the S800 focal plane [34]. HiRA consisted of 14 charged-particle detector telescopes set up 35 cm from the target with angular coverage between  $8^\circ$  and  $40^\circ$  in the laboratory frame. Each HiRA telescope contained a 65- $\mu\text{m}$ , single-sided, 32-strip  $\Delta E$  silicon detector, a 1500- $\mu\text{m}$ , double-sided, 32-strip  $E$  silicon detector, and an array of four 3.9-cm-thick CsI(Tl) scintillator crystals, with each crystal spanning roughly one quadrant of the preceding silicon detectors. The HiRA detectors were calibrated with radioactive sources and energy-loss calculations as described in Ref. [35].

Using the energy deposited in the  $\Delta E$ ,  $E$ , and CsI(Tl) detectors, deuterons were identified in HiRA using the standard  $\Delta E$ - $E$  technique. Reaction residues were identified in the S800 focal plane detectors using energy loss and

time-of-flight information. Two Microchannel Plates (MCPs) designated as MCP0 (1 m upstream from the target) and MCP1 (10 cm upstream from the target) counted the incoming beam particles. These MCPs also tracked the beam position for each event in order to improve the angular resolution [36].

After gating on the  $^{46,34}\text{Ar}(p, d)^{45,33}\text{Ar}$  reaction channels, the excitation energy of the heavy recoil nucleus was reconstructed. Figures 1(a) and 1(b) show excitation energy spectra for  $^{33}\text{Ar}$  and  $^{45}\text{Ar}$  with peaks corresponding to various final states in each argon recoil. We extracted the ground-state-to-ground-state angular distributions by fitting and integrating the ground-state peaks for many angular slices. At forward angles, the standard deviations of the energy spectra are 240 keV for  $^{33}\text{Ar}$  and 260 keV for  $^{45}\text{Ar}$ . The resolution was slightly worse for the  $^{46}\text{Ar}$  beam despite the thinner target because the beam spot was significantly larger than for the  $^{34}\text{Ar}$  beam. Separate diagnostic runs with each beam using a thick carbon target indicated negligible background from carbon-induced reactions. The ground-state peak for  $^{33}\text{Ar}$  (corresponding to an  $l = 0$  transfer) is clearly distinguishable from the first-excited state at  $E^* = 1.359$  MeV. In the  $^{45}\text{Ar}$  case, we separate contributions from the  $f_{7/2}$  ground state ( $l = 3$  transfer) and  $p_{3/2}$  first-excited state ( $l = 1$  transfer,  $E^* = 0.542$  MeV) by focusing on forward angles where the cross section of the  $l = 1$  transfer is expected to be highest. Figure 1(b) shows a clear distortion of the ground-state peak due to contribution from the  $p_{3/2}$  state. As there are no other states in this energy range in  $^{45}\text{Ar}$ , we are able to fit these spectra with a double-Gaussian function where the width of each Gaussian is fixed to 260 keV. The best-fit centroids correspond closely with the expected energies.

The absolute cross-section normalization was determined using MCP1. Figures 1(c) and 1(d) show the resulting differential cross-section data in the center-of-mass (c.m.) frame as well as corresponding adiabatic distorted wave approximation (ADWA) calculations for the pure single-neutron transfer into the  $^{33}\text{Ar}$  ground state and both the ground state and first-excited state of  $^{45}\text{Ar}$ . The corresponding data are given in Tables I and II. The lines in each figure show ADWA calculations performed with the TWOFNR code using two separate optical potentials. The first potential is the CH89 global optical model, which is a parametrized fit across data from many different reactions, and uses a conventional Woods-Saxon form for the neutron-bound-state potential [37]. The data for this fit range from 10 to 65 MeV, close to the presently considered beam energy of 70 MeV. The second approach uses the JLM optical model which is microscopically calculated from convoluted nucleon-density distributions for a specific reaction system [38]. In this case, the densities were calculated via a Hartree-Fock (HF) approach using the SkX Skyrme parametrization [39]. We adjust the radius parameter of the bound-state orbital to reproduce the mean-squared radius from the HF calculation as described in Ref. [13]. The rms neutron radii for  $^{34}\text{Ar}$  and  $^{46}\text{Ar}$  were 3.121 and 3.559 fm, respectively. This latter cross-section calculation method is referred to below as “JLM + HF.”

Consideration of momentum matching is important to ensure the validity of the one-step distorted wave Born approximation used in the ADWA calculations. The product

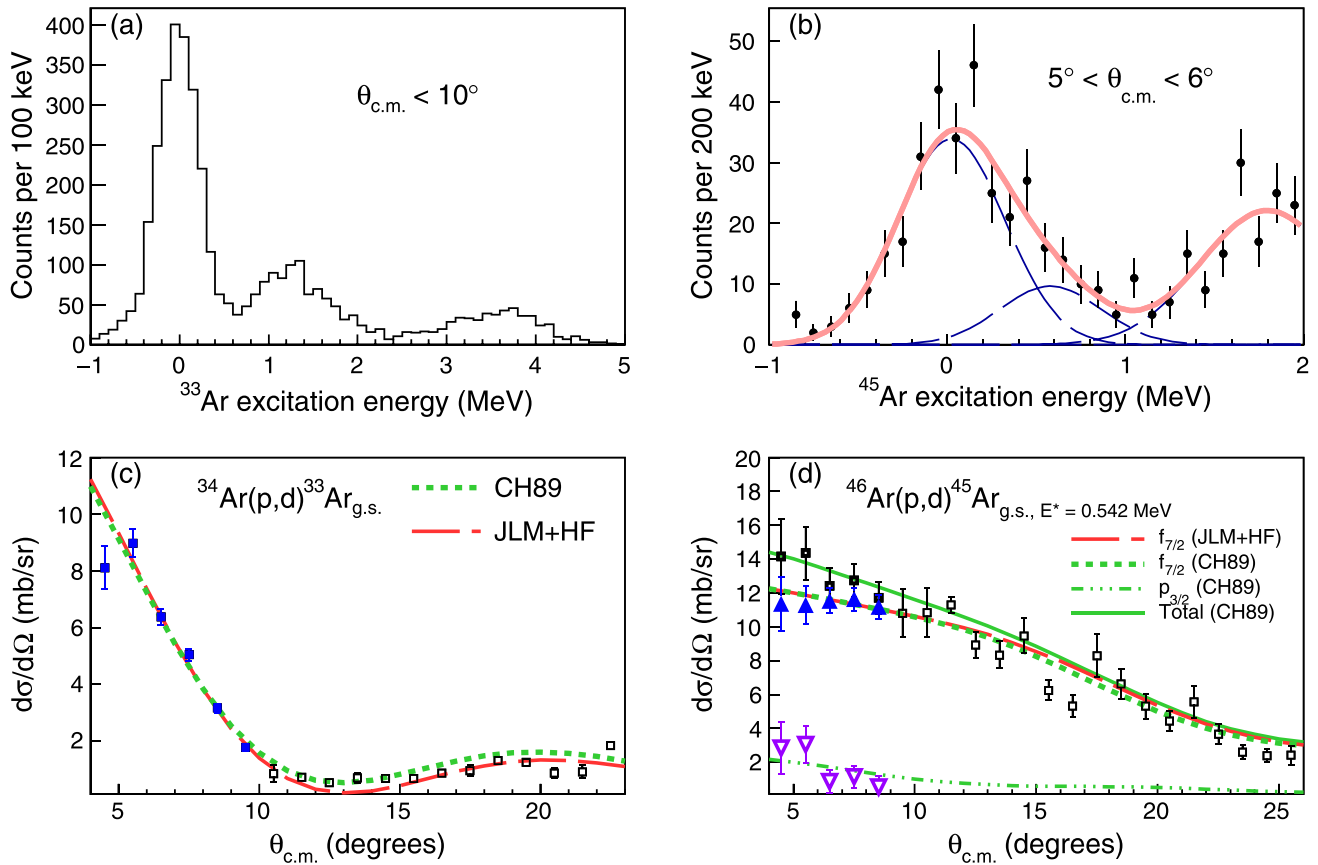


FIG. 1. Example excitation energy spectra for (a)  $^{34}\text{Ar}(p,d)^{33}\text{Ar}$  with a  $\theta_{\text{c.m.}}$  (the c.m. reaction angle) cut of less than  $10^\circ$ , and (b)  $^{46}\text{Ar}(p,d)^{45}\text{Ar}$  for  $\theta_{\text{c.m.}}$  between  $5^\circ$  and  $6^\circ$ . In the latter case, each individual state is modeled using a fixed-width Gaussian (dashed, blue lines), and the total fit is shown by the red, solid line. [(c) and (d)] Differential cross sections for these two reactions, as well as corresponding ADWA reaction calculations scaled with the SFs to match the data. The blue, solid cross-section points in each plot indicate the data used for SF extraction. In (d), the black, square points correspond to the combined cross section of the  $^{45}\text{Ar}$  ground state and first-excited state. At forward angles, contributions from the ground state and first-excited state can be separated (shown as the upward-facing, blue triangles and the downward-facing, purple triangles, respectively).

of the momentum transfer  $q$  and the radius  $R$  at which the transfer reaction occurs should be close (within  $1-2 \hbar$ ) to the orbital angular-momentum transfer [21]. A beam energy of 70 MeV gives  $qR$  of 1.6 and 2.6 for the  $^{34}\text{Ar}(p,d)$  and  $^{46}\text{Ar}(p,d)$  reactions, respectively, and in both cases the values are within reasonable distance of the transferred orbital angular momentum.

Figure 1(c) shows scaled ADWA calculations for  $^{34}\text{Ar}(p,d)^{33}\text{Ar}_{\text{g.s.}}$  using both the CH89 and JLM + HF approaches (the green dotted and red dashed lines, respectively). Figure 1(d) shows scaled CH89 and JLM + HF calculations for transfer to the  $^{45}\text{Ar}$  ground state (again, the green dotted and red dashed lines), and a CH89 calculation for transfer to the first-excited state (green dash-dotted line). There is no JLM + HF cross-section calculation for the first-excited state of  $^{45}\text{Ar}$  because this requires HF calculations of the nucleon density. Each calculated cross section is scaled with the corresponding extracted SF (as described below).

Given reasonable agreement in the cross-section shape, the experimental SF is the best-fit scaling factor (determined by  $\chi^2$  minimization) between the ADWA calculation and

the experimental data. Extracted SFs are given in Table III. Uncertainty is calculated by combining in quadrature the 10% uncertainty from the  $\chi^2$  minimization with 10% overall normalization uncertainty (determined by studying the stability of the beam normalization over the course of the experiment) to get 14% total uncertainty on each point. For the  $^{34}\text{Ar}$  case, we extract the SF from the prominent peak using the six points at the most forward angles (from  $4^\circ$  to  $10^\circ$  in the c.m. frame). The  $^{46}\text{Ar}$  cross section does not have any sharp peaks, and we instead do a  $\chi^2$  minimization across the five most forward-angle points (from  $4^\circ$  to  $9^\circ$  in the c.m. frame) where we can separate the ground-state peak from the low-lying  $p_{3/2}$  excited state using the previously described fits. The cross sections to the ground state and first-excited state of  $^{45}\text{Ar}$  are shown in Fig. 1(d) (by the solid, blue triangles and open, purple triangles, respectively) and given in Table II. The sum of these two contributions yields the bold, open, black squares. For angles greater than  $9^\circ$  the cross section for both states (black, open squares) is determined by a single Gaussian fit. The sum of the two scaled CH89 calculations is shown by the solid, green line.

TABLE I. Differential cross sections (and associated uncertainties) for  $^{34}\text{Ar}(p, d)^{33}\text{Ar}$  and  $^{46}\text{Ar}(p, d)^{45}\text{Ar}$  into both the ground state and first-excited state in the center-of-mass frame.

Angle ( $^\circ$ )	$d\sigma/d\Omega$ (mb/sr)	
	$^{34}\text{Ar}(p, d)^{33}\text{Ar}_{\text{g.s.}}$	$^{46}\text{Ar}(p, d)^{45}\text{Ar}_{\text{g.s.}+p_{3/2}}$
4.5	$8.11 \pm 0.77$	$14.17 \pm 2.20$
5.5	$8.98 \pm 0.49$	$14.36 \pm 1.57$
6.5	$6.38 \pm 0.29$	$12.42 \pm 1.02$
7.5	$5.03 \pm 0.21$	$12.75 \pm 0.95$
8.5	$3.15 \pm 0.16$	$11.72 \pm 0.97$
9.5	$1.75 \pm 0.12$	$10.79 \pm 1.42$
10.5	$0.82 \pm 0.29$	$10.85 \pm 1.42$
11.5	$0.71 \pm 0.08$	$11.31 \pm 0.48$
12.5	$0.51 \pm 0.07$	$8.94 \pm 0.78$
13.5	$0.69 \pm 0.18$	$8.34 \pm 0.80$
14.5	$0.65 \pm 0.07$	$9.47 \pm 1.05$
15.5	$0.66 \pm 0.07$	$6.25 \pm 0.58$
16.5	$0.86 \pm 0.09$	$5.32 \pm 0.68$
17.5	$0.94 \pm 0.17$	$8.29 \pm 1.27$
18.5	$1.29 \pm 0.10$	$6.61 \pm 0.91$
19.5	$1.23 \pm 0.13$	$5.33 \pm 0.75$
20.5	$0.84 \pm 0.17$	$4.42 \pm 0.58$
21.5	$0.90 \pm 0.25$	$5.55 \pm 0.95$
22.5		$3.64 \pm 0.60$
23.5		$2.60 \pm 0.42$
24.5		$2.39 \pm 0.41$
25.5		$2.41 \pm 0.56$

### III. REDUCTION FACTORS

The reduction factor for each final state is defined as the ratio of the experimental SF to the large-basis shell model (LBSM) calculation,  $\text{SF(LBSM)}$ . Table III shows the results for the ground-state transfer from  $^{34}\text{Ar}$  and  $^{46}\text{Ar}$  using both the JLM + HF and CH89 analyses. Figure 2 shows the reduction factors plotted against  $\Delta S$  for both the JLM + HF (top panel) and CH89 (bottom panel) cases in comparison with low-energy transfer data from Ref. [19] and the Be/C-induced knockout data [16,40] for  $^{46}\text{Ar}$ ,  $^{34}\text{Ar}$ , and  $^{32}\text{Ar}$ . Although the magnitude of the individual transfer-reaction reduction factors changes depending on the analysis approach (as discussed in Ref. [13]), the slopes of the best-fit linear trends (indicated by the dashed lines) are consistent. The best linear fit for the

TABLE II. Differential cross sections (and associated uncertainties) for  $^{46}\text{Ar}(p, d)^{45}\text{Ar}$  in the center-of-mass frame for both the ground state and first-excited state.

Angle ( $^\circ$ )	$d\sigma/d\Omega$ (mb/sr)	
	$^{46}\text{Ar}(p, d)^{45}\text{Ar}_{\text{g.s.}}$	$^{46}\text{Ar}(p, d)^{45}\text{Ar}_{p_{3/2}}$
4.5	$11.35 \pm 1.58$	$2.82 \pm 1.53$
5.5	$11.31 \pm 1.13$	$3.05 \pm 1.09$
6.5	$11.55 \pm 0.75$	$0.87 \pm 0.70$
7.5	$11.63 \pm 0.69$	$1.12 \pm 0.65$
8.5	$11.18 \pm 0.71$	$0.54 \pm 0.67$

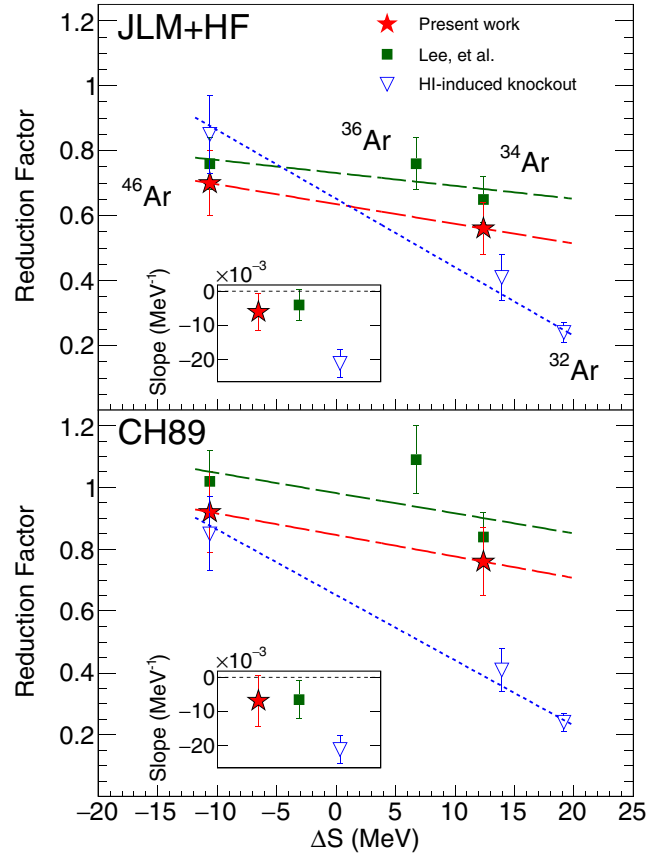


FIG. 2. Asymmetry dependence of reduction factors for 70 MeV/nucleon transfer (the present work, red stars), 33 MeV/nucleon transfer from [19] (green squares), and Be/C-induced knockout (open blue triangles) on argon isotopes for the transfer points were extracted using the JLM + HF (top panel) and CH89 (bottom panel) models, as described in the text. The red and green dashed lines correspond to the best linear fits for the 70 MeV/nucleon and 33 MeV/nucleon transfer points, respectively, and the dotted blue line is the best linear fit for the knockout points. The slopes from each fit are shown in the inset plots. The  $\Delta S$  values for the  $^{34}\text{Ar}$  points vary slightly because the knockout measurement was inclusive, as opposed to the exclusive transfer measurements.

Be/C-induced knockout data is shown as a blue, dotted line. Inset plots illustrate the slope parameters from each fit: in all transfer-reaction analyses, the slopes with respect to  $\Delta S$  are less steep than the slope of the Be/C-induced knockout data.

Slopes from reduction-factor data provide a simple and model-independent metric for asymmetry dependence for different experimental and theoretical approaches. Figure 3 plots the slope parameters from linear fits of reduction factors and the associated uncertainties (given by the colored bands) for the transfer, Be/C-induced knockout, ( $e, e'p$ ), and ( $p, pN$ ) techniques. The blue, Be/C-induced knockout band was calculated via a linear fit of all the data from the seminal compilation by Tostevin and Gade and more recent data from Flavigny *et al.* on oxygen isotopes [8,17]. The blue triangle is from a fit using only argon isotopes [16,40]. The green,

TABLE III. Extracted spectroscopic factors and reduction factors for both  $^{34}\text{Ar}$  and  $^{46}\text{Ar}$ .

Isotope	$l_j^\pi$	$\Delta S$ (MeV)	(Theo.)	(Expt.)		(Expt.)		HF RMS radius (fm)
			SF(LBSM)	SF(CH89)	$R_s$ (CH89)	SF(JLM+HF)	$R_s$ (JLM+HF)	
$^{34}\text{Ar}$	$s_{1/2}^+$	12.40	1.31	$1.00 \pm 0.14$	$0.76 \pm 0.11$	$0.73 \pm 0.10$	$0.56 \pm 0.08$	3.121
$^{46}\text{Ar}$	$f_{7/2}^-$	-10.63	5.16	$4.77 \pm 0.67$	$0.92 \pm 0.13$	$3.59 \pm 0.50$	$0.70 \pm 0.10$	3.559

horizontally striped ( $e, e'p$ ) bands are extracted from two analyses of the NIKHEF measurements, with the results from Kramer *et al.* on the left and those from Lapikas *et al.* on the right [5,6]. They are presented with the caveat that both of these studies only include stable isotopes and therefore do not cover a wide asymmetry range. The red, diagonally striped transfer bands represent the  $\Delta S$  dependence from several transfer-reaction measurements, including a compilation by Xu *et al.* (leftmost red band) [22] and measurements of oxygen isotopes across a wide asymmetry range by Flavigny *et al.* (rightmost red band) [20]. The red star corresponds to the slope from a linear fit using transfer-reaction data on argon isotopes only (from both the JLM + HF results presented here and the earlier low-energy measurements [19]). The central transfer band (adjacent to the star) incorporates the present JLM + HF reduction factors with a previous compilation of similarly analyzed data [41,42]. The gold, vertically striped quasifree knockout bands correspond to separate analyses of data from oxygen, carbon, and nitrogen measurements [both ( $p, 2p$ ) and ( $p, pn$ )]. In order from left to right, the bands show results from Phuc *et al.*, Gomez-Ramos *et al.*, Holl *et al.*, and Atar *et al.* [14,23–25]. Each of these works employed different theoretical models to extract the SFs, and all exhibit similar asymmetry trends. Together, results from transfer, ( $e, e'p$ ), and ( $p, 2p$ ) and ( $p, pn$ ) experiments indicate a weaker asymmetry dependence than what is observed in knockout reactions using beryllium and carbon targets.

The rightmost column of Fig. 3 shows the  $\Delta S$  dependence of spectroscopic factors obtained from several theoretical calculations, indicated by black lines and labeled in the legend [43–46]. Coupled-cluster calculations from Jensen *et al.*

treat bound states and continuum states on equal footing, and ascribe the observed weak quenching to many-body correlations from neutron scattering states [43]. Self-consistent Green's function (SCGF) results from Barbieri *et al.* using the Faddeev Random Phase Approximation (FRPA) attempt to account for both short- and long-range correlation effects, and exhibit weak asymmetry dependence [44]. Cipollone *et al.* also find weak quenching by using the SCGF approach to evaluate the impact of three-nucleon forces on spectroscopic factors [46]. The theoretical model showing the strongest asymmetry dependence calculated radial overlap functions with a nonstandard inhomogeneous equation, and calibrated the effective nucleon-nucleon interaction using asymptotic normalization coefficients [45]. Even this approach, however, does not reproduce the magnitude of the quenching seen in the Be/C-induced knockout data.

Slope values for all experimental and theoretical studies are provided in Table IV, as well as the number of data points used for the fit.

Experimental evidence for strong asymmetry dependence has so far only been observed in Be/C-induced knockout reaction data. Considering the large quantity of knockout results on beryllium and carbon targets that consistently show this effect, it is possible that the theoretical knockout model may be incomplete. It could be that the eikonal approximation neglects absorptive processes that uniquely affect deeply bound

TABLE IV. Reduction-factor slope parameters for a variety of experimental and theoretical approaches.

Method	References	Slope ( $\text{MeV}^{-1}$ )	Points
Transfer <sup>a</sup>	[42]	$0.0014 \pm 0.0021$	33
Transfer	[22]	$-0.00086 \pm 0.0025$	21
Transfer	[20]	$-0.0004 \pm 0.0027$	7
( $p, pN$ )	[14]	$-0.0033 \pm 0.0020$	5
( $p, pN$ )	[24]	$-0.0059 \pm 0.0013$	15
( $p, pN$ )	[23]	$-0.0024 \pm 0.0012$	14
( $p, pN$ )	[25]	$-0.0024 \pm 0.0031$	18
Knockout (Be/C)	[8,17]	$-0.016 \pm 0.00040$	34
( $e, e'p$ )	[6,13]	$-0.0070 \pm 0.0037$	10
( $e, e'p$ )	[5]	$0.0045 \pm 0.0052$	8
( $e, e'p$ )	[52]	$-0.012 \pm 0.0038$	2
SCGF (3NFs) <sup>b</sup>	[46]	$-0.000072$	15
SCGF (FRPA) <sup>b</sup>	[44]	$-0.0019$	13
DOM <sup>b</sup>	[53]	$-0.0057$	11
Coupled cluster <sup>b</sup>	[43]	$-0.0068$	10
Inhomogenous <sup>b</sup>	[45]	$-0.010$	31

<sup>a</sup>Includes the present work.

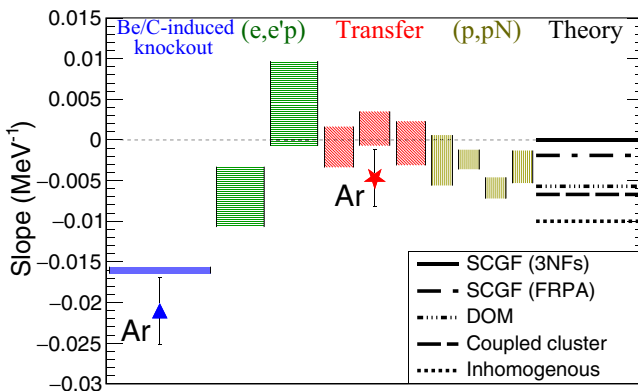
<sup>b</sup>Theoretical nuclear structure calculations.


FIG. 3. A summary of reduction-factor slope parameters across different techniques. Details are provided in the text, and the slope values can be found in Table IV with corresponding citations.

nucleons [17,47], the influence of core excitations [48,49], or a combination of these and other effects. A recent update to the aforementioned Tostevin and Gade compilation of Be/C-induced knockout results shows no significant difference from the original trend, despite including measurements with beam energies up to 1.6 GeV/nucleon [18]. Another study found that the systematics described by Tostevin and Gade do not hold for several cases of Be-induced knockout with particle-unstable residuals, suggesting the influence of continuum coupling or dynamical effects [50].

To be complete, however, we note that Atkinson *et al.* have reanalyzed the NIKHEF data for  $^{40}\text{Ca}$  and  $^{48}\text{Ca}$  using dispersive optical model (DOM) potentials [51,52]. The resulting slope is  $-0.012 \pm 0.004 \text{ MeV}^{-1}$ , which indicates a stronger dependence than all techniques except for Be/C-induced knockout. We refrain from including this slope in Fig. 3 since the two points only cover a small range of asymmetry near stability. Further DOM analysis of other NIKHEF measurements is needed. A previous DOM analysis by Charity *et al.* that featured 11 calcium isotopes is included in Fig. 3 and Table IV [53].

Recent work on electron scattering data demonstrates that nucleons have a strong preference to form correlated neutron-proton high momentum pairs in the nucleus [26]. To understand how these neutron-proton pairs influence asymmetry dependence, Paschalis *et al.* explicitly calculated the impact of such short-range correlations (SRC) on the reduction factor as a function of asymmetry using two distinct linear models to account for differences in SRC effects on neutrons and protons [27]. The resulting asymmetry dependence is again weak compared to the quenching seen in the Be/C-induced knockout data.

#### IV. CONCLUSION

In conclusion, 70 MeV/nucleon transfer reaction measurements on unstable argon isotopes show much weaker reduction factor asymmetry dependence than what is seen in Be/C-induced knockout results. The available experimental and theoretical evidence generally indicate a weak but nonzero asymmetry dependence, although the error bars from some measurements do overlap with a slope of  $0 \text{ MeV}^{-1}$ . Agreement between the high-energy transfer measurements shown here and previous low-energy measurements from Ref. [19] provides evidence that transfer reactions can be reliably employed to study asymmetric systems at high beam energies for spectroscopic studies when appropriate momentum matching conditions are satisfied [54]. The transfer reaction probe can be further understood via measurements with the high-asymmetry beams that will be available at next-generation accelerators like the Facility for Rare Isotope Beams.

#### ACKNOWLEDGMENTS

The authors thank the operations staff of the NSCL for experimental support. The authors also thank J. Tostevin for use of the TWOFNR program. This work was supported by the National Science Foundation under Grant No. PHY-1565546. This material is based on work supported by the U.S. Department of Energy, Office of Science, Office of Nuclear Science, under Award No. DE-FG02-94ER40848 and DE-FG02-87ER-40316. J.M. was supported by a Department of Energy National Nuclear Security Administration Stewardship Science Graduate Fellowship under cooperative Agreement No. DE-NA0002135.

- 
- [1] W. Dickhoff and C. Barbieri, *Prog. Part. Nucl. Phys.* **52**, 377 (2004).
- [2] L. B. Weinstein, E. Piasezky, D. W. Higinbotham, J. Gomez, O. Hen, and R. Shneor, *Phys. Rev. Lett.* **106**, 052301 (2011).
- [3] A. Akmal, V. R. Pandharipande, and D. G. Ravenhall, *Phys. Rev. C* **58**, 1804 (1998).
- [4] C. Barbieri, *Phys. Rev. Lett.* **103**, 202502 (2009).
- [5] L. Lapikás, *Nucl. Phys. A* **553**, 297 (1993).
- [6] G. Kramer, H. Blok, and L. Lapikás, *Nucl. Phys. A* **679**, 267 (2001).
- [7] J. Lee, M. B. Tsang, W. G. Lynch, M. Horoi, and S. C. Su, *Phys. Rev. C* **79**, 054611 (2009).
- [8] J. A. Tostevin and A. Gade, *Phys. Rev. C* **90**, 057602 (2014).
- [9] M. B. Tsang, J. Lee, and W. G. Lynch, *Phys. Rev. Lett.* **95**, 222501 (2005).
- [10] M. B. Tsang, J. Lee, S. C. Su, J. Y. Dai, M. Horoi, H. Liu, W. G. Lynch, and S. Warren, *Phys. Rev. Lett.* **102**, 062501 (2009).
- [11] J. P. Schiffer, C. R. Hoffman, B. P. Kay, J. A. Clark, C. M. Deibel, S. J. Freeman, A. M. Howard, A. J. Mitchell, P. D. Parker, D. K. Sharp, and J. S. Thomas, *Phys. Rev. Lett.* **108**, 022501 (2012).
- [12] F. Flavigny, N. Keeley, A. Gillibert, and A. Obertelli, *Phys. Rev. C* **97**, 034601 (2018).
- [13] J. Lee, J. A. Tostevin, B. A. Brown, F. Delaunay, W. G. Lynch, M. J. Saelim, and M. B. Tsang, *Phys. Rev. C* **73**, 044608 (2006).
- [14] L. Atar, S. Paschalis, C. Barbieri, C. A. Bertulani, P. Díaz Fernández, M. Holl, M. A. Najafi, V. Panin, H. Alvarez-Pol, T. Aumann, V. Avdeichikov, S. Beceiro-Novo, D. Bemmerer, J. Benlliure, J. M. Boillos, K. Boretzky, M. J. G. Borge, M. Caamaño, C. Caesar, E. Casarejos, K. Zuber *et al.* (R<sup>3</sup>B Collaboration), *Phys. Rev. Lett.* **120**, 052501 (2018).
- [15] T. Aumann, C. Barbieri, D. Bazin, C. Bertulani, A. Bonaccorso, W. Dickhoff, A. Gade, M. Gómez-Ramos, B. Kay, A. Moro, T. Nakamura, A. Obertelli, K. Ogata, S. Paschalis, and T. Uesaka, *Prog. Part. Nucl. Phys.* **118**, 103847 (2021).
- [16] A. Gade, D. Bazin, B. A. Brown, C. M. Campbell, J. A. Church, D. C. Dinca, J. Enders, T. Glasmacher, P. G. Hansen, Z. Hu, K. W. Kemper, W. F. Mueller, H. Olliver, B. C. Perry, L. A. Riley, B. T. Roeder, B. M. Sherrill, J. R. Terry, J. A. Tostevin, and K. L. Yurkewicz, *Phys. Rev. Lett.* **93**, 042501 (2004).
- [17] F. Flavigny, A. Obertelli, A. Bonaccorso, G. F. Grinyer, C. Louchart, L. Nalpas, and A. Signoracci, *Phys. Rev. Lett.* **108**, 252501 (2012).
- [18] J. A. Tostevin and A. Gade, *Phys. Rev. C* **103**, 054610 (2021).
- [19] J. Lee, M. B. Tsang, D. Bazin, D. Coupland, V. Henzl, D. Henzlova, M. Kilburn, W. G. Lynch, A. M. Rogers, A. Sanetullaev, A. Signoracci, Z. Y. Sun, M. Youngs, K. Y. Chae, R. J. Charity, H. K. Cheung, M. Famiano, S. Hudan, P. O'Malley, W. A. Peters *et al.*, *Phys. Rev. Lett.* **104**, 112701 (2010).

- [20] F. Flavigny, A. Gillibert, L. Nalpas, A. Obertelli, N. Keeley, C. Barbieri, D. Beaumel, S. Boissinot, G. Burgunder, A. Cipollone, A. Corsi, J. Gibelin, S. Giron, J. Guillot, F. Hammache, V. Lapoux, A. Matta, E. C. Pollacco, R. Raabe, M. Rejmund *et al.*, *Phys. Rev. Lett.* **110**, 122503 (2013).
- [21] B. P. Kay, J. P. Schiffer, and S. J. Freeman, *Phys. Rev. Lett.* **111**, 042502 (2013).
- [22] Y. Xu, D. Pang, X. Yun, C. Wen, C. Yuan, and J. Lou, *Phys. Lett. B* **790**, 308 (2019).
- [23] M. Gómez-Ramos and A. Moro, *Phys. Lett. B* **785**, 511 (2018).
- [24] M. Holl, V. Panin, H. Alvarez-Pol, L. Atar, T. Aumann, S. Beceiro-Novo, J. Benlliure, C. Bertulani, J. Boillos, K. Boretzky, M. Caamaño, C. Caesar, E. Casarejos, W. Catford, J. Cederkall, L. Chulkov, D. Cortina-Gil, E. Cravo, I. Dillmann, P. D. Fernández *et al.*, *Phys. Lett. B* **795**, 682 (2019).
- [25] N. Tri Toan Phuc, K. Yoshida, and K. Ogata, *Phys. Rev. C* **100**, 064604 (2019).
- [26] O. Hen, M. Sargsian, L. B. Weinstein, and E. Piasezky, *Science* **346**, 614 (2014).
- [27] S. Paschalis, M. Petri, A. Macchiavelli, O. Hen, and E. Piasezky, *Phys. Lett. B* **800**, 135110 (2020).
- [28] K. Wimmer, *J. Phys. G: Nucl. Part. Phys.* **45**, 033002 (2018).
- [29] P. Hansen and J. Tostevin, *Annu. Rev. Nucl. Part. Sci.* **53**, 219 (2003).
- [30] P. Alons, J. Kraushaar, and P. Kunz, *Phys. Lett. B* **137**, 334 (1984).
- [31] R. Anderson, J. Kraushaar, J. Shepard, and J. Comfort, *Nucl. Phys. A* **311**, 93 (1978).
- [32] J. Manfredi, Asymmetry dependence of spectroscopic factors: A study of transfer reactions on argon isotopes at 70 MeV/u, Ph.D. thesis, Michigan State University, East Lansing, MI, 2018.
- [33] M. Wallace, M. Famiano, M.-J. van Goethem, A. Rogers, W. Lynch, J. Clifford, F. Delaunay, J. Lee, S. Labostov, M. Mocko, L. Morris, A. Moroni, B. Nett, D. Oostdyk, R. Krishnasamy, M. Tsang, R. de Souza, S. Hudan, L. Sobotka, R. Charity *et al.*, *Nucl. Instrum. Methods A* **583**, 302 (2007).
- [34] D. Bazin, J. Caggiano, B. Sherrill, J. Yurkon, and A. Zeller, *Nucl. Instrum. Methods B* **204**, 629 (2003).
- [35] J. Manfredi, J. Lee, W. Lynch, C. Niu, M. Tsang, C. Anderson, J. Barney, K. Brown, Z. Chajecski, K. Chan, G. Chen, J. Estee, Z. Li, C. Pruitt, A. Rogers, A. Sanetullaev, H. Setiawan, R. Showalter, C. Tsang, J. Winkelbauer *et al.*, *Nucl. Instrum. Methods A* **888**, 177 (2018).
- [36] A. Rogers, A. Sanetullaev, W. Lynch, M. Tsang, J. Lee, D. Bazin, D. Coupland, V. Henzl, D. Henzlova, M. Kilburn, M. Wallace, M. Youngs, F. Delaunay, M. Famiano, D. Shapira, K. Jones, K. Schmitt, and Z. Sun, *Nucl. Instrum. Methods A* **795**, 325 (2015).
- [37] R. Varner, W. Thompson, T. McAbee, E. Ludwig, and T. Clegg, *Phys. Rep.* **201**, 57 (1991).
- [38] J.-P. Jeukenne, A. Lejeune, and C. Mahaux, *Phys. Rev. C* **16**, 80 (1977).
- [39] B. A. Brown, *Phys. Rev. C* **58**, 220 (1998).
- [40] A. Gade, P. Adrich, D. Bazin, M. D. Bowen, B. A. Brown, C. M. Campbell, J. M. Cook, T. Glasmacher, P. G. Hansen, K. Hosier, S. McDaniel, D. McGlinchery, A. Obertelli, K. Siwek, L. A. Riley, J. A. Tostevin, and D. Weisshaar, *Phys. Rev. C* **77**, 044306 (2008).
- [41] J. Lee, M. B. Tsang, and W. G. Lynch, *Phys. Rev. C* **75**, 064320 (2007).
- [42] H. Lee, Survey of neutron spectroscopic factors and asymmetry dependence of neutron correlations in transfer reactions, Ph.D. thesis, Michigan State University, East Lansing, MI, 2010.
- [43] O. Jensen, G. Hagen, M. Hjorth-Jensen, B. A. Brown, and A. Gade, *Phys. Rev. Lett.* **107**, 032501 (2011).
- [44] C. Barbieri and W. H. Dickhoff, *Int. J. Mod. Phys. A* **24**, 2060 (2009).
- [45] N. K. Timofeyuk, *Phys. Rev. Lett.* **103**, 242501 (2009).
- [46] A. Cipollone, C. Barbieri, and P. Navrátil, *Phys. Rev. C* **92**, 014306 (2015).
- [47] R. Shane, R. J. Charity, L. G. Sobotka, D. Bazin, B. A. Brown, A. Gade, G. F. Grinyer, S. McDaniel, A. Ratkiewicz, D. Weisshaar, A. Bonaccorso, and J. A. Tostevin, *Phys. Rev. C* **85**, 064612 (2012).
- [48] C. Louchart, A. Obertelli, A. Boudard, and F. Flavigny, *Phys. Rev. C* **83**, 011601(R) (2011).
- [49] Y. L. Sun, J. Lee, Y. L. Ye, A. Obertelli, Z. H. Li, N. Aoi, H. J. Ong, Y. Ayyad, C. A. Bertulani, J. Chen, A. Corsi, F. Cappuzzello, M. Cavallaro, T. Furono, Y. C. Ge, T. Hashimoto, E. Ideguchi, T. Kawabata, J. L. Lou, Q. T. Li *et al.*, *Phys. Rev. C* **93**, 044607 (2016).
- [50] R. J. Charity, L. G. Sobotka, and J. A. Tostevin, *Phys. Rev. C* **102**, 044614 (2020).
- [51] M. C. Atkinson, H. P. Blok, L. Lapikás, R. J. Charity, and W. H. Dickhoff, *Phys. Rev. C* **98**, 044627 (2018).
- [52] M. Atkinson and W. Dickhoff, *Phys. Lett. B* **798**, 135027 (2019).
- [53] R. J. Charity, J. M. Mueller, L. G. Sobotka, and W. H. Dickhoff, *Phys. Rev. C* **76**, 044314 (2007).
- [54] R. Johnson, E. Stephenson, and J. Tostevin, *Nucl. Phys. A* **505**, 26 (1989).